Nanoscale

Accepted Manuscript

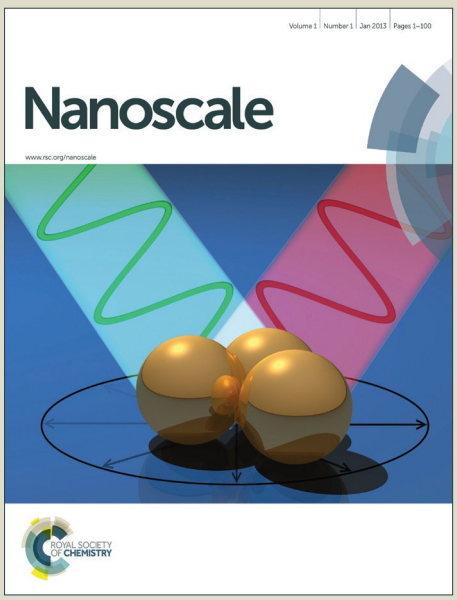

ROYAL SOCIETY OF CHEMISTRY

www.rsc.org/nanoscale

Nanoscale

ARTICLE

Solution-Based Synthesis and Purification of Zinc Tin Phosphide Nanowires†

Received 00th January 20xx,
Accepted 00th January 20xx

DOI: 10.1039/x0xx00000x

www.rsc.org/

Erik J. Sheets,[a] Robert B. Balow,[b] Wei-Chang Yang,[c] Eric A. Stach,[d] and Rakesh Agrawal*[a]

The solution-based synthesis of nanoscale earth-abundant semiconductors has the potential to unlock simple, scalable, and tunable material processes which currently constrain development of novel compounds for alternative energy devices. One such promising semiconductor is zinc tin phosphide ($ZnSnP_2$). We report the synthesis of $ZnSnP_2$ nanowires via a solution-liquid-solid mechanism utilizing metallic zinc and tin in decomposing trioctylphosphine (TOP). Dried films of the reaction product are purified of binary phosphide phases by annealing at 345 °C. Tin is removed using a 0.1 M nitric acid treatment leaving pure $ZnSnP_2$ nanowires. Diffuse reflectance spectroscopy indicates $ZnSnP_2$ has a direct bandgap energy of 1.24 eV which is optimal for solar cell applications. Using a photoelectrochemical cell, we demonstrate cathodic photocurrent generation at open circuit conditions from the $ZnSnP_2$ nanowires upon solar simulated illumination confirming p-type conductivity.

Introduction

The search for earth abundant, non-toxic solar absorption materials has brought attention to a myriad of zinc-blende and chalcopyrite based compounds with I_2-II-IV-VI_4 and I_3-V-VI_4 stoichiometries such as $Cu_2ZnSn(S,Se)_4$, $Cu_3P(S,Se)_4$, and Cu_3AsS_4 among others.[1,2] Meanwhile, cubic III-V semiconductors including GaAs and InP, although highly efficient, have not seen large scale application due to a combination of high material costs, expensive fabrication, and susceptibility to defect impurities.[3] Bridging the gap between earth abundant II-IV-VI materials and efficient III-V materials, $ZnSnP_2$ has been theorized to exhibit ideal physical and optical characteristics for solar cell applications.[4] All the elements Zn, Sn, and P exist in abundance in the earth's crust and $ZnSnP_2$ is thought to be a safe semiconducting material.[5] It has been observed to have a direct bandgap with values in the ideal range of 1.32-1.53 eV for single junction solar cells.[6] However, use of $ZnSnP_2$ in solar devices has proven difficult predominantly due to current synthesis techniques.

Bulk $ZnSnP_2$ crystals are generally grown by slow heating and cooling dilute solutions of Zn, P, or ZnP_2 in a Sn melt.[6–8] This method is very slow, time consuming, and rather cumbersome.[9] Growth by liquid phase epitaxy on GaAs at relatively high temperatures is not suitable for growth of thin films on glass substrates for large scale production.[10] $ZnSnP_2$ films have also been grown through vapor phase deposition methods where a mixture of H_2, Zn-metal vapor, and toxic PH_3 is passed over SnO_2 thin films at high temperatures.[11] $ZnSnP_2$ grown by ultrahigh vacuum evaporation of elements Zn, Sn, and red-P on quartz substrates resulted in visibly inhomogeneous films.[9] Use of gas source molecular beam epitaxy to grow $ZnSnP_2$ on GaAs resulted in $ZnSnP_2$ regions consisting of a nano-scale mixture of $ZnSnP_2$ and $ZnSnAs_2$.[12] The "tin-flux" method uses temperatures in excess of 600 °C with cooling rates of 3 °C/h. The use of high temperatures and long times needed make this method unsuitable for growing $ZnSnP_2$ on commonly used substrates such as glass.[5] The use of highly toxic tris-trimethylsilylphosphine with Zn and Sn halides in conjunction with high temperatures of 600 °C has also been reported.[13] There is a need for a method with lower processing temperatures that allows use of commonly used substrates and is easy to scale while producing high quality $ZnSnP_2$.

[a] School of Chemical Engineering, Purdue University 480 Stadium Mall Drive. West Lafayette, IN 47907.
[b] Department of Chemistry, Purdue University 560 Oval Drive. West Lafayette, IN 47907.
[c] School of Materials Engineering, Purdue University 701 Stadium Avenue. West Lafayette, IN 47907.
[d] Center for Functional Nanomaterials, Brookhaven National Laboratory, 2 Center Street, Upton, NY 11973

†Electronic Supplementary Information (ESI) available: characterization details, synthesis of Zn_3P_2 and Sn_4P_3, GC-MS, $ZnSnP_2$ optimization experiments, diffuse reflectance calculations, Rietveld refinement, $ZnSnP_2$ SAED, TEM EDS data, and TGA data. See DOI: 10.1039/x0xx00000x

The known methods in the literature either produce bulk crystals at the millimeter scale or epitaxially grow thin films on GaAs substrates. To date, there is no known method to synthesize nanometer size $ZnSnP_2$ particles using solution-based chemistry for subsequent use in various applications. Chalcogenide nanoparticles have been used to make solar cells with nanostructures and nanoparticle inks to fabricate conventional thin film solar cells.[14–16] Here our goal is to create a similar opportunity of $ZnSnP_2$ by synthesizing nanometer sized $ZnSnP_2$ particles via a simple solvent-based reaction method. We report a successful synthesis of $ZnSnP_2$ nanowires using a solution-liquid-solid (SLS) reaction in trioctylphosphine (TOP). By initially forming a melt phase consisting of Zn and Sn in the presence of decomposing trioctylphosphine, $ZnSnP_2$ precipitates out as the saturation limit within the melt phase is exceeded. Binary Zn and Sn phosphides are removed by annealing, and the resultant Sn is then removed by a nitric acid treatment. The p-type $ZnSnP_2$ nanowires are isolated and exhibit a direct bandgap of 1.24 eV, ideal for photovoltaic applications. The $ZnSnP_2$ nanowires generate a photocurrent under solar simulated illumination, thus providing evidence for their potential as an earth abundant solar absorption material.

Results and Discussion

Trioctylphosphine as a phosphorus source

The use of TOP as a phosphorus source has become popular in solution-based nanocrystal synthesis techniques due to its versatility as a solvent,[17] as a stabilizing capping ligand (often in the presence of trioctylphosphine oxide),[18–20] as a strong reducing agent,[21] and as a phosphorus source for the synthesis of numerous transition metal phosphides.[22–26] Of particular interest, Zn_3P_2 has been synthesized using TOP as the phosphorus source with bulk Zn[22] or with highly flammable dimethyl zinc,[27] forming mono-disperse nanocrystals in the latter. Tin phosphides are known to exist as either SnP, SnP_3, Sn_3P_4, and Sn_4P_3,[28–32] but interestingly, only $SnP_{(0.94)}$ has been synthesized from TOP as a phosphorus source to date.[33] The precondition for the synthesis of such metal phosphides from TOP appears to be the presence of a metal which catalyzes the P-C scission for decomposition to take place at a high enough temperature.[22] Otherwise TOP will boil without self-decomposing.

Experiments utilizing precursor Zn or Sn nanoparticles heated in TOP (individually) to the decomposition temperature (365-370 ^{o}C) for 5 h produced Zn_3P_2 and Sn_4P_3 respectively with no indication of the original metallic precursors by X-ray diffraction (XRD) (ESI†). Combining stoichiometric ratios of Zn and Sn nanoparticle precursors together in TOP with similar heating not only produced Zn_3P_2 and Sn_4P_3 as expected but also produced the target material $ZnSnP_2$ as seen in Figure 1. XRD clearly shows the coexistence of all three distinct phases implying the oxidation of the metal precursors by the reduction of TOP during the decomposition reaction. Gas chromatography mass spectrometry (GC-MS) of the supernatant confirmed the presence of TOP derivatives, supporting this hypothesis (ESI†).

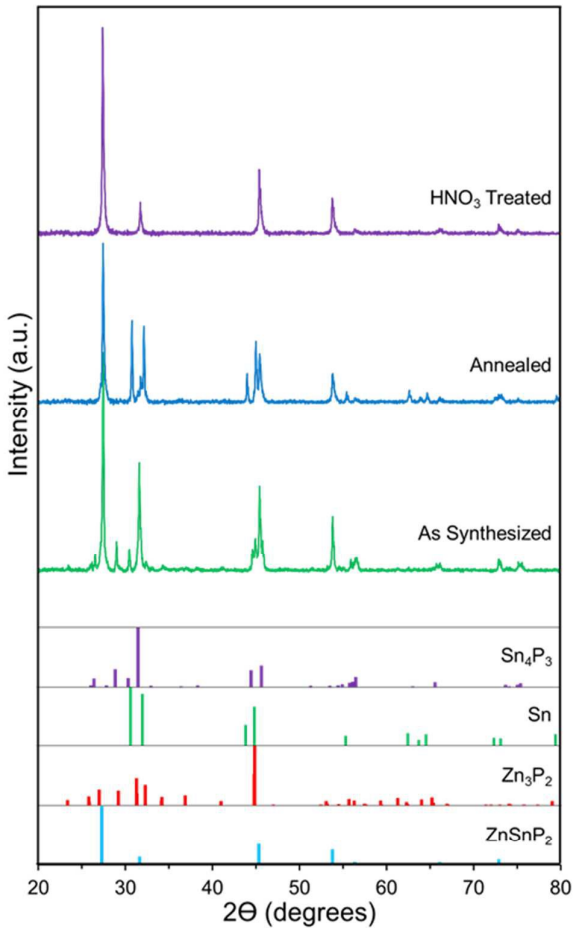

Fig. 1 XRD patterns of processed $ZnSnP_2$ samples showing the removal of Sn_4P_3 and Zn_3P_2 by annealing and removal of Sn by treating with 0.1 M nitric acid. The reference XRD patterns have been included for Sn_4P_3 (PDF# 01-071-2221), Sn (PDF# 4-673), Zn_3P_2 (PDF# 01-073-4212), and tetragonal $ZnSnP_2$ (PDF# 73-396).

Synthesis Product Analysis and Mechanism Proposal

The standard reaction utilizing stoichiometric quantities of Zn and Sn produced 56.2(±0.3)% $ZnSnP_2$, 32.6(±0.7)% Zn_3P_2, and 11.2(±0.3)% Sn_4P_3. Pure phase $ZnSnP_2$ was not obtained by varying the molar ratios of Zn:Sn. Larger molar quantities of Zn compared to Sn increased the relative quantity of Zn_3P_2 while decreasing the quantity of Sn_4P_3 and $ZnSnP_2$. Conversely, adding larger molar quantities of Sn increased the quantity of Sn_4P_3 compared to Zn_3P_2 and $ZnSnP_2$. The optimal stoichiometric Zn:Sn ratio was thus kept at 1:1 in order to maximize the relative intensity of $ZnSnP_2$ compared to the binary phosphides (ESI†).

Analysis of the product from the initial reaction of Zn, Sn, and TOP via transmission electron microscopy (TEM) and scanning transmission electron microscopy (STEM) with energy dispersive X-ray spectroscopy (EDS) (Figure 2) showed evidence of crystal growth by a SLS mechanism: analogous to

vapor-liquid-solid (VLS) growth.[34] The tell-tale sign of such SLS growth is a spherical head capping a tail of a different crystal structure as seen in Figure 2-E. The head consists of Sn with trace Zn, and the tail consists of Zn_3P_2 and/or $ZnSnP_2$ which transitions at various lengths in the nanowires as phosphorus is incorporated. An example of this transition is explored in Figure 3-A where the approximate stoichiometric ratios are shown from TEM EDS analysis. The head is clearly Sn-rich with a trace amount of Zn and P. The mid-tail section approximates stoichiometric $ZnSnP_2$ while the deep tail approximates Zn_3P_2. Tail lengths have been observed on the micron scale while widths are <200 nm and have been observed as small as 10 nm.

We infer that the reaction mechanism begins with the melting of the Sn nanopowder in TOP (230 °C). As the temperature increases, so does the solubility of Zn in Sn, consistent with the eutectic binary phase diagram. As TOP catalytically decomposes, phosphorus reacts with the alloyed ZnSn spheres. As the temperature of the reaction relaxes due to the lower boiling point of the decomposition products, the metal precursors become saturated until Zn, Zn_3P_2, or $ZnSnP_2$ precipitate out as nanowires.[35] If Zn precipitates out first, it will quickly react with phosphorus, forming Zn_3P_2. Any excess Sn not involved in forming $ZnSnP_2$ reacts with TOP separately

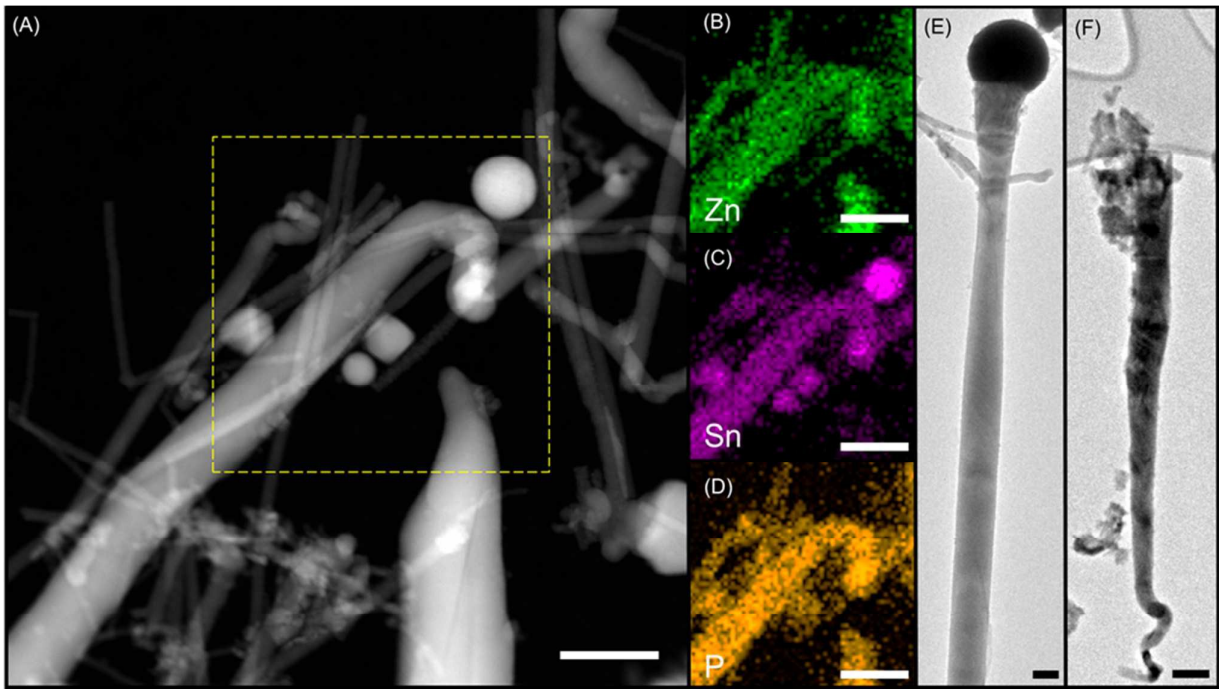

Fig. 2 (A) STEM image of the as-synthesized product from heating Zn and Sn nanopowders in TOP. (B-D) STEM EDS elemental maps of Zn, Sn, and P confirming the multiple phases present: $ZnSnP_2$, Zn_3P_2, Sn_4P_3, and Sn. (E) TEM image of the synthesis product growth by SLS where the head of Sn caps a rod of $ZnSnP_2$ and Zn_3P_2. (F) TEM image after annealing and treating the $ZnSnP_2$ with nitric acid emphasizing the loss of the Sn head seen after synthesis. Scale bar represents 100 nm in all images.

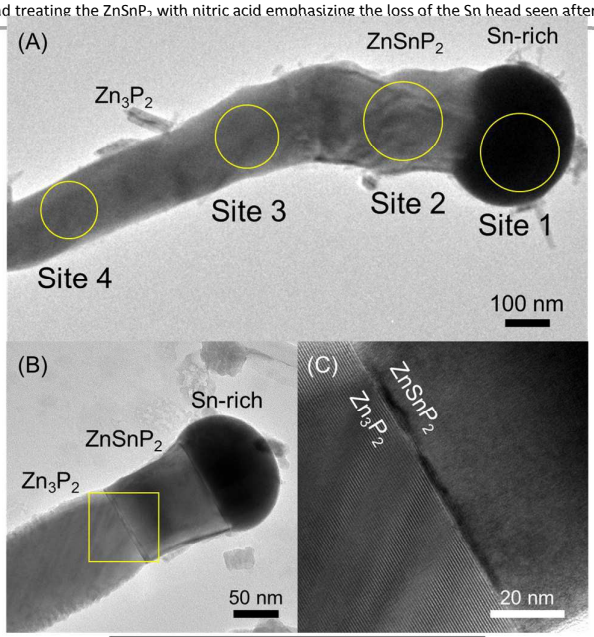

Mol. Ratio	Zn/P	Sn/P	(Zn+Sn)/P
Site 1	1.47	16.2	17.7
Site 2	0.50	0.57	1.06
Site 3	1.38	0.01	1.39
Site 4	1.29	0.00	1.29

to form Sn_4P_3. The reason Zn or Zn_3P_2 occasionally precipitates out prior to $ZnSnP_2$ is particularly intriguing considering the similarity in crystal structure[36] as observed in Figure 3-B,C and is subsequently explored.

In an effort to provide further evidence of our proposed mechanism, Zn nanowires have successfully been synthesized by heating a 1:1 molar ratio of Zn:Sn nanopowders in 1-octadecene to 310 °C (just below its boiling point) without the presence of a phosphorus source (TOP). After 1 h, the mixture was cooled and the product analyzed via TEM. As expected, Zn nanowires were observed in the product (ESI†) indicating that the Zn was soluble in the Sn, precipitating out as the solubility limit was reached upon cooling. TEM EDS indicated the nanowire's Zn/Sn atomic ratio was 15.9, concluding the wire is essentially Zn. The increasing diameter of the Zn nanowires as a function of length is similar to that which is observed in the standard $ZnSnP_2$ synthesis using TOP and is evidence of a small

initial nucleation site followed by an increasing growth. An example of the Zn nanowires can be seen in Figure ESI-9. Although no images explicitly showed Sn heads connected to the Zn nanowires, the flat ends of the nanowires are indicative of a broken interface likely caused in the sample washing and dispersion process.

Fig. 3 (A) TE
head (Site 1)
(Site 2), and
between ZnS

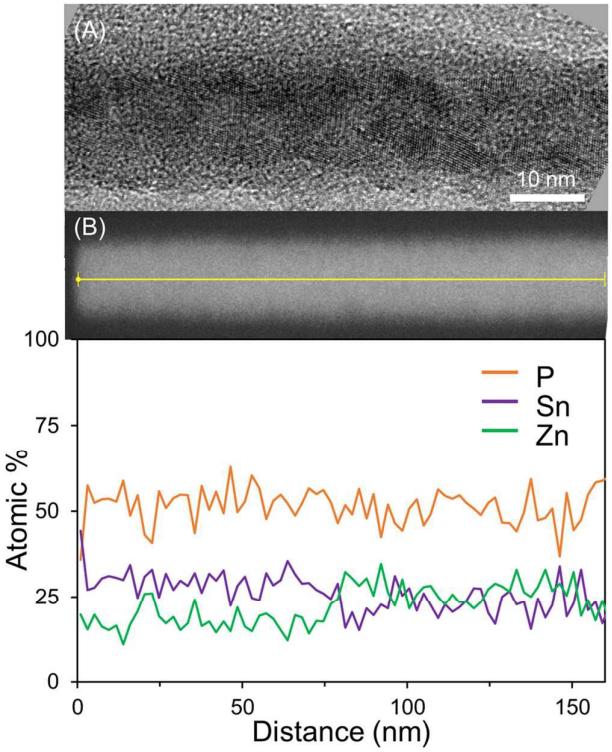

Fig. 4 (A) HR TEM image of a $ZnSnP_2$ nanowire after annealing and nitric acid treatment showing the wire is a single crystal. (B) STEM EDS linescan of a $ZnSnP_2$ nanowire after annealing and nitric acid treatment. Atomic fractions of Zn, Sn, and P are constant throughout the rod and approximate the ideal stoichiometric ratio of 1:1:2.

The significance of observing Zn nanowires in this experiment prove that Zn can precipitate out of a Zn-Sn melt phase, and we conjecture that in the presence of decomposing TOP, the Zn nanowires will react to form Zn_3P_2. Thus, in the standard $ZnSnP_2$ synthesis, an initial Zn nanowire may precipitate out of the Zn-Sn melt as the system temperature drops upon decomposition of TOP, causing an initial Zn_3P_2 nanowire. As the reaction continues and more phosphorus is incorporated into the melt phase, conditions favor the transition to $ZnSnP_2$ which can be grown at the same nucleation site as the Zn_3P_2 due to the similar crystal lattices. Direct nucleation of Zn_3P_2 from the Zn-Sn melt phase cannot be explicitly ruled out by this experiment, but a more sophisticated in-situ analysis is required to make a definitive conclusion.

Purification of $ZnSnP_2$

To isolate pure $ZnSnP_2$ from its binary phosphide derivatives, an annealing step and nitric acid treatment were implemented in succession. Zn_3P_2 is known to vaporize above 347 °C by a congruent decomposition reaction which produces $Zn_{(g)}$ and $P_{(g)}$.[37] From our own investigations, Sn_4P_3 also decomposes above 400 °C into $Sn_{(l)}$ and $P_{(g)}$ (ESI†). Keeping this temperature in mind, the as-synthesized $ZnSnP_2$ was drop cast from an ethanol-based dispersion onto a glass substrate and annealed at 345 °C in a tube furnace for 12 h while flowing 100 sccm Ar. The resulting films were analyzed by XRD and were void of any

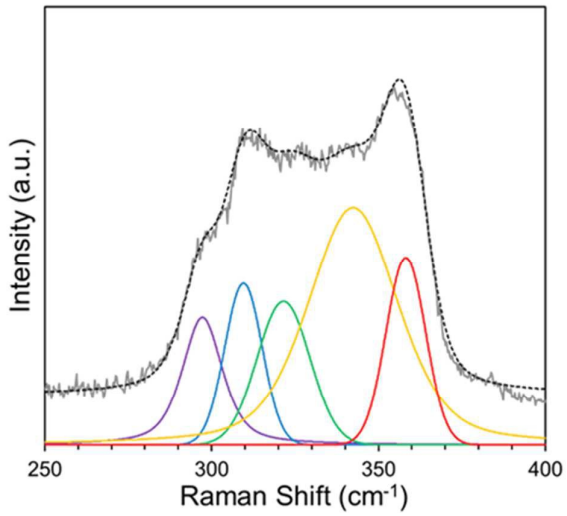

Fig. 5 Raman spectroscopy of acid treated $ZnSnP_2$ confirming its phase purity and a mixed sphalerite-chalcopyrite crystal structure as compared to Mintairov et al. The grey line is the obtained spectrum while the dashed line is the summation of the multi-colored fitted peaks from a linear combination of Gaussian and Lorenzian curves.

Zn_3P_2 and Sn_4P_3. $ZnSnP_2$ remained in the film with metallic Sn, indicating that the binary metal phosphides are volatile at that temperature (see Figure 1).

After annealing, pure $ZnSnP_2$ is attained by removing residual Sn using nitric acid.[6] While submerging the annealed films in 0.1 M nitric acid for 6 h with slow stirring, Sn reacts with the nitric acid, precipitating SnO_2 which is rinsed off of the films with water upon removal from the acid. Because film quality is typically reduced following acid treatment (by creating pin holes), the resulting product is scraped off and washed with water before being recast on glass for further analysis.

XRD suggests no impurity phases are present in the acid treated film and confirms the chalcopyrite-based crystal structure (Figure 1). $ZnSnP_2$ is well known to occur in two coordination states: an ordered tetragonal chalcopyrite phase and a disordered cubic sphalerite phase (theoretical band gaps 1.70 and 0.75 eV respectively).[4,38] By comparing relative XRD peak intensities across the cubic (F-32m (216), PDF# 01-071-6473) and tetragonal (I-42d (122), PDF# 73-396) phases, approximate mole fractions of each can be estimated using Rietveld refinement. The main difference between the two isomorphic phases are extra peaks that appear in the tetragonal phase in addition to those observed in the cubic phase. Using Rietveld refinement on the XRD of our final $ZnSnP_2$ product, we have determined 55.6(±0.5) % by weight is the ordered chalcopyrite phase and 44.4(±0.3) % is the disordered sphalerite phase (ESI†).

Scanning electron spectroscopy (SEM) EDS confirms overall atomic ratios for a large volume of product approximate expected values: Zn/P = 0.53, Sn/P = 0.55, Zn/Sn = 1.05. Individual nanowires were analyzed by high resolution TEM and shown to be single crystals (Figure 4-A). STEM EDS linescan across a nanowire showed atomic uniformity and elemental ratio near 1:1:2 (Zn:Sn:P) as seen in Figure 4-B. The acid treated product contains neither Sn heads nor binary phosphide impurities.

Additional evidence of the overall purity has been observed using Raman spectroscopy as seen in Figure 5.

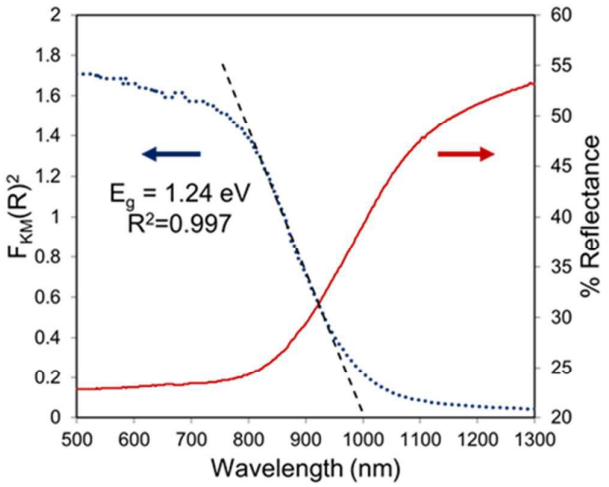

Fig. 6 Diffuse reflectance measurements (right) taken on acid treated ZnSnP2 indicate a sharp transition between 800 and 1100 nm. To determine the bandgap of ZnSnP2, a Tauc plot (left) of the diffuse reflectance data was made using the Kubelka-Munk function for a direct energy transition. Extrapolation of the linear region to the x-axis reveals the bandgap to be 1003 nm (1.24 eV) with an excellent fit.

Results were compared to the vibrational Raman experiments conducted by Mintairov et al.[39] Fitting the observed Raman spectrum with a linear combination of Gaussian and Lorentzian distributions revealed 5 distinct peaks at 297, 310, 322, 342, and 358 cm^{-1}. The peaks at 310 and 358 cm^{-1} coincide with expected peaks from the ordered chalcopyrite structure, while peaks at 297, 322, and 342 cm^{-1} are consistent with the disordered sphalerite system. These results agree with our Rietveld refinement analysis concluding the obtained product is a mixed ordered-disordered chalcopyrite-sphalerite system. No other peaks corresponding to impurity phases such as Zn_3P_2,[40] ZnP_2,[41] or others were observed.

Band Gap Analysis

The bandgap of the synthesized and purified $ZnSnP_2$ was determined using diffuse reflectance. Reflection data was transposed using the Kubelka-Munk function[42] and analyzed on a Tauc plot to estimate the energy of transition between energy bands. Figure 6 shows the original reflectance data collected as a function of wavelength with a distinct transition between 800 and 1100 nm. Extrapolation of the linear regions of the Tauc plot to the x-intercept yields the approximate energy of band transitions.[43] A direct transition was observed at 1.24 eV. Experimentally observed direct bandgaps in literature have varied from 1.68-1.64 eV for the ordered chalcopyrite phase down to 1.38-1.25 eV for the disordered sphalerite phase.[44–46] Our data are consistent with literature and show $ZnSnP_2$ nanowires have a band gap in the optimal energy region for solar absorption in homojunction device.[47]

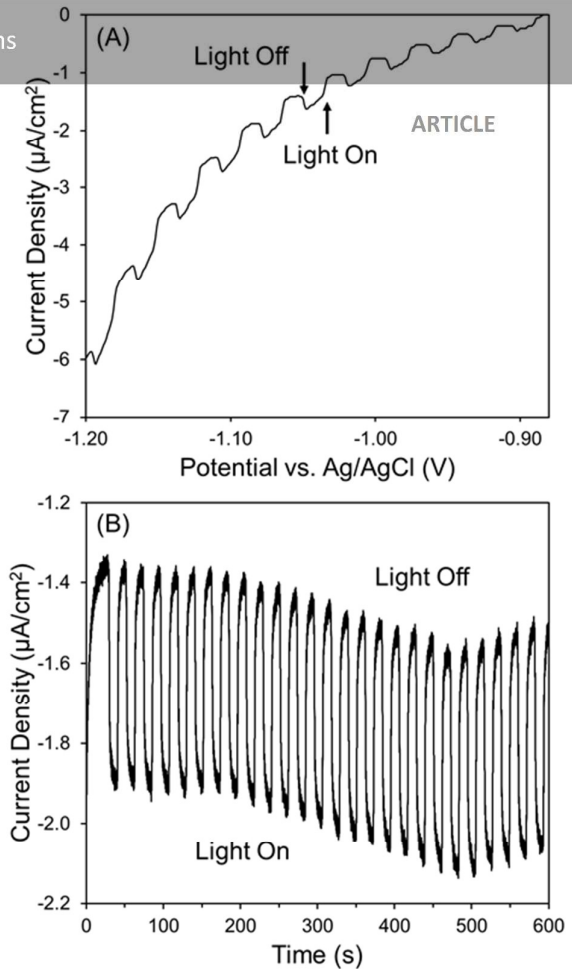

Fig. 7 (A) Linear sweep voltammetry of $ZnSnP_2$ on ITO. The photoelectrode is back illuminated using interrupted solar simulated light (AM1.5G, 100mW/cm^2) in 0.5 M Na_2S (pH 12). A maximum photocurrent density is obtained near -1.1 V vs. Ag/AgCl. (B) $ZnSnP_2$ photoresponse under -1.1 V bias (vs. Ag/AgCl) for 600 s with a cathodic photocurrent density of 0.58 μA/cm^2.

Photoresponse

In an initial proof of concept experiment, the $ZnSnP_2$ nanocrystals were evaluated for photoresponse under solar simulated AM1.5G (100 mW/cm^2) light in 0.5 M Na_2S (adjusted to pH 12.0 with HCl). The $ZnSnP_2$ working electrode was fabricated by drop casting from ethanol onto a 150 nm tin-doped indium oxide (ITO) on glass substrate. The cast films were annealed at 250 °C under N_2 for 15 min to increase adherence to the substrate. The $ZnSnP_2$ photoelectrode was back-illuminated with on and off cycled light showing both light and dark behavior of the $ZnSnP_2$ film. To measure the current-potential response, linear sweep voltammetry (LSV) was performed at a rate of 10 mV/s from open circuit conditions showing increasing cathodic photocurrent generation with increasing bias (Figure 7-A). The robustness of the $ZnSnP_2$ nanowire thin films was evaluated by cycling light on and off while applying a bias of -1.1 V vs. Ag/AgCl over 10 min with a stable photocurrent of generation of approximately 0.6 μA/cm^2 (Figure 7-B). The current generated in the dark is

likely from electrochemical reduction of the redox couple (S^{2-} /S_n^{2-}) and not photocorrosion of the $ZnSnP_2$ nanocrystals as evidenced by the stable photocurrent generation throughout the scan.

Conclusions

$ZnSnP_2$ nanowires have been synthesized from metallic Zn and Sn through a SLS growth mechanism with decomposing trioctylphosphine. The method also synthesizes Zn_3P_2 and Sn_4P_3. Binary phosphide impurities were removed by annealing. Residual Sn was removed using a nitric acid treatment. The final product was shown to be impurity free with a direct bandgap of 1.24 eV and a stable cathodic photocurrent density of 0.58 μA/cm^2 upon solar simulated illumination in 0.5 M Na_2S at a bias of -1.1 V vs. Ag/AgCl. The synthesis method described provides a simple, solvent-based, scalable route to $ZnSnP_2$ nanowires without the use of time consuming, high temperature, or vacuum-based techniques. Thus, $ZnSnP_2$ is a viable earth-abundant photovoltaic device candidate with new potential as a nanocrystalline material.

Materials and Methods

Solution-based synthesis

0.5 mmol of Zn (Sigma-Aldrich, >99%, < 50nm) and 0.5 mmol Sn (Sigma-Aldrich, 99.7%, < 150 nm) nanopowders are added to a two neck round-bottom flask with a condenser followed by 20 mmol TOP (Sigma-Aldrich, 90%) under nitrogen in a glovebox. The flask is then sealed using Apeizon H vacuum grease and attached to a standard Schlenk line apparatus where it is purged three times at room temperature with argon (Indiana Oxygen, 99.97%). The contents are heated to 370 oC in 20 min. As the temperature approaches 370 oC (about 360 oC), TOP begins to decompose, producing a white vapor.‡ The temperature subsequently relaxes slowly to 280 oC over the course of 5 h without changing the heating source input. Upon cooling the contents to room temperature, the product is washed four times using 1:1 v/v toluene and ethanol (200 proof) followed by centrifugation at 14,000 rpm for 5 min. Films of the product are cast on 1 in. square glass substrates from ethanol.

Annealing and Acid Treatments

The as-cast films are placed in the center of a purged, vertical, 3-zone tube furnace and annealed at 345 ^{o}C for 12 h under 100 sccm Ar. The samples are cooled naturally to room temperature. The films are placed in a petri dish and submerged under at least 20 ml 0.1 M nitric acid (Macron) solution with slow stirring for 6 h. The films of $ZnSnP_2$ are dried in air after rinsing with ultrapure water (18.2 MΩ·cm, Millipore).

Characterization

Products and intermediate phases were analysed utilizing the following characterization techniques and instruments: X-ray diffraction using a Rigaku SmartLab (room temperature, Cu K_α radiation), Raman spectroscopy using a Horiba/Jobin-Yvon LabRAM HR800, (scanning) transmission electron microscopy ((S)TEM) using a FEI Tecnai 20 (200 kV), and field emission scanning electron spectroscopy energy dispersive X-ray spectroscopy (FE-SEM EDS) using a FEI Quanta 3D FEG Dual-beam microscope. The initial reaction's supernatant was analysed for decomposition products by GC-MS using an Agilent 5975C. The final $ZnSnP_2$ films were analysed for photoactivity by photoelectrochemical (PEC) measurements using a Digi-Ivy D2011 single channel potentiostat equipped with a standard three-electrode system, details of which are found in the ESI†. Diffuse reflectance spectroscopy of the $ZnSnP_2$ films was performed using a Hitachi U-4100 UV-vis-NIR spectrophotometer (341-F). Specific analysis conditions, calculations, and sample preparation notes are found in the ESI†.

Acknowledgements

The authors would like to sincerely thank Professor Sreeram Vaddiraju and Venkata Vasiraju of Texas A&M for their insightful discussions and assistance with collecting diffuse reflectance spectroscopy data, Ruihong Zhang for her assistance with STEM EDS data acquisitions, Christopher Gilpin for his TEM guidance, and Karl Wood for his assistance in collecting the GC/MS data. This work was supported by the National Science Foundation's Solar Economy IGERT grant #0903670. E.A.S. acknowledges support to the U.S. DOE Office of Science Facility at Brookhaven National Laboratory under Contract No. DE-SC0012704.

Notes and references

‡ White phosphorus vapor is potentially toxic and flammable if released in air. Care must be taken when cleaning the glassware as phosphorus may accumulate near joints and begin to smoke or ignite.

1 V. Itthibenchapong, R. S. Kokenyesi, A. J. Ritenour, L. N. Zakharov, S. W. Boettcher, J. F. Wager and D. A. Keszler, *J. Mater. Chem. C*, 2013, **1**, 657.
2 R. B. Balow, E. J. Sheets, M. M. Abu-Omar and R. Agrawal, *Chem. Mater.*, 2015, **27**, 2290–2293.
3 M. van Schilfgaarde, T. J. Coutts, N. Newman and T. Peshek, *Appl. Phys. Lett.*, 2010, **96**, 143503.
4 D. O. Scanlon and A. Walsh, *Appl. Phys. Lett.*, 2012, **100**, 251911.
5 K. Nakatani, T. Minemura, K. Miyauchi, K. Fukabori, H. Nakanishi, M. Sugiyama and S. Shirakata, *Jpn. J. Appl. Phys.*, 2008, **47**, 5342–5344.
6 T. E. Warner, *Synthesis, Properties and Mineralogy of Important Inorganic Materials*, John Wiley & Sons, Inc., 2011.
7 C. H. L. Goodman, *Nature*, 1957, **197**, 828–829.
8 M. Rubenstein and R. W. Ure Jr., *J. Phys. Chem. Solids*, 1968, **29**, 551–555.

9 P. K. Ajmera, H. Y. Shin and B. Zamanian, *Sol. Cells*, 1987, **21**, 291–299.
10 G. A. Davis, M. W. Muller and C. M. Wolfe, *J. Cryst. Growth*, 1984, **69**, 141–148.
11 J. Sansregret, *Mater. Res. Bull.*, 1981, **16**, 607–611.
12 B. Lita, M. Beck, R. S. Goldman, G. Aa. Seryogin, S. A. Nikishin and H. Temkin, *Appl. Phys. Lett.*, 2000, **77**, 2894.
13 S. C. Goel, W. E. Buhro, N. L. Adolphi and M. S. Conradi, *J. Organomet. Chem.*, 1993, **449**, 9–18.
14 C.-H. M. Chuang, P. R. Brown, V. Bulović and M. G. Bawendi, *Nat. Mater.*, 2014, **13**, 796–801.
15 S. M. McLeod, C. J. Hages, N. J. Carter and R. Agrawal, *Prog. Photovoltaics Res. Appl.*, 2015, **23**.
16 C. K. Miskin, W.-C. Yang, C. J. Hages, N. J. Carter, C. Joglekar, E. A. Stach and R. Agrawal, *Prog. Photovoltaics Res. Appl.*, 2015, **23**, 654–659.
17 S. Chen, X. Zhang, Q. Zhang and W. Tan, *Nanoscale Res. Lett.*, 2009, **4**, 1159–1165.
18 D. V Talapin, A. L. Rogach, I. Mekis, S. Haubold, A. Kornowski, M. Haase and H. Weller, *Colloids Surfaces A Physicochem. Eng. Asp.*, 2002, **202**, 145–154.
19 A. J. Morris-Cohen, M. Malicki, M. D. Peterson, J. W. J. Slavin and E. A. Weiss, *Chem. Mater.*, 2012.
20 C. B. Murray, D. J. Noms and M. G. Bawendi, *J. Am. Chem. Soc.*, 1993, **115**, 8706–8715.
21 X. Hou, X. Zhang, S. Chen, Y. Fang, J. Yan, N. Li and P. Qi, *Appl. Surf. Sci.*, 2011, **257**, 4935–4940.
22 A. E. Henkes and R. E. Schaak, *Chem. Mater.*, 2007, **19**, 4234–4242.
23 P. K. Khanna, K.-W. Jun, K. B. Hong, J.-O. Baeg and G. K. Mehrotra, *Mater. Chem. Phys.*, 2005, **92**, 54–58.
24 R.-K. Chiang and R.-T. Chiang, *Inorg. Chem.*, 2007, **46**, 369–71.
25 J. Park, B. Koo, K. Y. Yoon, Y. Hwang, M. Kang, J.-G. Park and T. Hyeon, *J. Am. Chem. Soc.*, 2005, **127**, 8433–40.
26 Y. Vasquez, A. E. Henkes, J. Chris Bauer and R. E. Schaak, *J. Solid State Chem.*, 2008, **181**, 1509–1523.
27 E. J. Luber, H. Mobarok and J. M. Buriak, *ACS Nano*, 2013, **7**, 8136–8146.
28 O. Olofsson, *Acta Chem. Scand.*, 1970, **24**, 1153–1162.
29 J. Gullman, *J. Solid State Chem.*, 1990, **87**, 202–207.
30 H. L. Su, Y. Xie, B. Li, X. M. Liu and Y. T. Qian, 1999, **113**, 110–113.
31 S. Liu, S. Li, M. Li, L. Yan and H. Li, *New J. Chem.*, 2013, **37**, 827.
32 K. A. Kovnir, Y. V. Kolen'ko, S. Ray, J. Li, T. Watanabe, M. Itoh, M. Yoshimura and A. V. Shevelkov, *J. Solid State Chem.*, 2006, **179**, 3756–3762.
33 Y. Kim, H. Hwang, C. S. Yoon, M. G. Kim and J. Cho, *Adv. Mater.*, 2007, **19**, 92–96.
34 T. J. Trentler, K. M. Hickman, S. C. Goel, A. M. Viano, P. C. Gibbons and W. E. Buhro, *Science (80-.).*, 1995, **270**, 1791–1794.
35 F. Wang, A. Dong, J. Sun, R. Tang, H. Yu and W. E. Buhro, *Inorg. Chem.*, 2006, **45**, 7511–7521.
36 I. E. Zanin, K. B. Aleinikova, M. M. Afanasiev and M. Y. Antipin, *J. Struct. Chem.*, 2004, **45**, 844–848.
37 A. R. Schoonmaker, R. C. Venkitaraman and P. K. Lee, *J. Phys. Chem.*, 1967, **71**, 2676–2683.
38 A. A. Vaipolin, N. A. Goryunova, L. I. Kleshchinskii, G. V. Loshakova and E. O. Osmonov, *Phys. Status Solidi*, 1968, **29**, 435.
39 A. M. Mintairov and N. A. Sadchikov, *Phys. Rev. B*, 1999, **59**, 15197–15207.
40 J. Misiewicz, *J. Phys. Condens. Matter*, 1989, **1**, 9283–9299.
41 J. Baran, Y. A. Pasechnik, K. V. Shportko, M. Trzebiatowska-Gusowska and E. F. Venger, *J. Mol. Struct.*, 2006, **792-793**, 239–242.
42 V. Džimbeg-Malčić, Ž. Barbarić-Mikočević and K. Itrić, *Tech. Gaz.*, 2011, **18**, 117–124.
43 J. Tauc, *Mater. Res. Bull.*, 1968, **3**, 37–46.
44 P. St-Jean, G. A. Seryogin and S. Francoeur, *Appl. Phys. Lett.*, 2010, **96**, 231913.
45 M. A. Ryan, M. W. Peterson, D. L. Williamson, J. S. Frey, G. E. Maciel and B. A. Parkinson, *J. Mater. Res.*, 1987, **2**, 528–537.
46 S. Sahin, Y. O. Ciftci, K. Colakoglu and N. Korozlu, *J. Alloys Compd.*, 2012, **529**, 1–7.
47 W. Shockley and H. Queisser, *J. Appl. Phys.*, 1961, **32**, 510–519.